ASTRONOMY & ASTROPHYSICS
SUPPLEMENT SERIES

Astron. Astrophys. Suppl. Ser. **144**, 509–515 (2000)

Experimental transition probabilities in NII lines

S. Mar, C. Pérez, V.R. González, M.A. Gigosos, J.A. del Val[1], I. de la Rosa, and J.A. Aparicio

Departamento de Optica, Facultad de Ciencias, Universidad de Valladolid, 47071 Valladolid, Spain
[1] Permanent address: Departamento de Física Aplicada, Universidad de Salamanca, E. Politécnica Superior 05071 Avila, Spain

Received February 15; accepted April 11, 2000

Abstract. This work reports an extensive collection of 108 transition probabilities of NII lines in the visible spectral region, all of them measured in an emission experiment. Relative intensity measurements have been made on a pulsed discharge lamp and the absolute A_{ki} values have been obtained by using the literature available data. Electron density and temperature range in this experiment from 0.2 to 1.1 10^{23} m^{-3} and from 17000 to 29000 K respectively. The first one has been simultaneously determined from two-wavelength interferometry and from the Stark broadening of HeI 471.3 nm, the second from Boltzmann-plot of NII lines and from NII/NI intensities ratios. The results are compared with the recent available literature.

Key words: atomic data — line: profile — methods: laboratory

1. Introduction

Nitrogen is among the most abundant elements in the universe. For the estimation of stellar chemical abundances the determination of radiative transition probabilities is of primary interest. Knowledge of the spectrum of singly ionised nitrogen is clearly required for the understanding of the associated plasmas. Moreover, it is frequently used in laboratory studies and in industrial applications. Although during the last decade, much theoretical effort has been devoted to advanced atomic structure calculation which provided such radiation data for NII (part of the Opacity Project), some accurate experimental data are still required (a) to establish with confidence the uncertainties of advanced calculations and (b) to settle especially the question to what degree LS coupling is applicable for the individual line strengths in this spectrum. According to Wiese et al. (1996) there is a lack of experimental data which are accurate enough to sensitively test the calculated results. Recently Musielok et al. 1996, have reported A_{ki} values for a fairly large number of lines (52) of the 3s−3p and 3p−3d transition arrays of NII with a wall-stabilized arc source. One of the aims of the present work is just to provide in only one experiment a great amount of data. These will be compared with the most recent literature. Furthermore, this experiment gives A_{ki} values for 13 NII spectral lines not collected in previous works, at least to the authors's knowledge.

All the results were obtained from measurements performed in a linear discharge lamp, where a mixture of helium and nitrogen was prepared so that self-absorption effects were negligible. The plasma source employed provides not only all kind of interferometric and spectroscopic registers with great reproducibility in different discharges, but also makes it possible in a broad range of electron density and temperature values. This allows us to acquire some reliable spectra for weak or non-isolated lines, otherwise very difficult to obtain.

In the present work absolute A_{ki} values have been obtained from relative intensity measurements taking as reference values the A_{ki} data available in the last NIST critical compilation (Wiese et al. 1996). In this way, we have determined NII excitation temperatures from Boltzmann-plots, and also temperatures given from NII/NI intensities ratios. The very good agreement between the two methods suggests that the plasma is well described by a partial local thermodynamic equilibrium (pLTE) model. The absence of self-absorption and the spectral calibration have been very carefully taken into account. The number of measurements (15) performed for each line along the plasma life, and its very controlled features, allows us to obtain a very good A_{ki} value by the mean value, and its uncertainty by the standard deviation (usually around 10%).

2. Experimental arrangement

The experimental set-up (shown in Fig. 1) and the methods have already been described in Gigosos et al. (1994),

Send offprint requests to: S. Mar

Aparicio et al. (1997, 1998). Here we summarize the specific details corresponding to the present experiment.

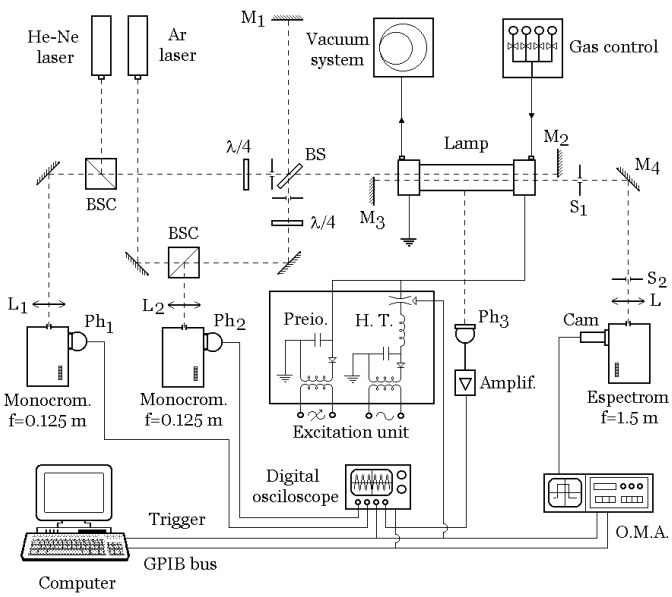

Fig. 1. Experimental set-up

The source of plasma consists of a cylindrical tube of Pyrex glass with 175 mm in length and 19 mm in interior diameter. The lamp has been designed to avoid sputtering as much as possible. The plasmas were created by discharging a capacitor bank of 20 μF charged up to 7.5 kV. During the whole experiment the lamp was working with a continuous flow of a mixture of helium and nitrogen, at a rate of 10 cm^3/min and 5 cm^3/min respectively and a global pressure of 1340 Pa. In these conditions, the NII emission lasts around 200 μs. The gas was pre-ionised in order to obtain the best discharge reliability. Spectroscopic and interferometric end-on measurements have been made simultaneously through the plasma life, and have been taken 2 mm off the lamp axis, and from symmetrical positions referred to it. The high axial homogeneity and the very good cylindrical symmetry of electron density and temperature in this lamp allows this (del Val et al. 1998).

According to Fig. 1, the lamp is placed in one of the arms of a Twyman-Green interferometer simultaneously illuminated with an argon ion laser (488.0 nm) and by an He-Ne laser (632.8 nm). The spectroscopic beam is directed (3 mm pinholes S1, S2, separated 1.5 m) and focused (cylindrical lens L with 150 mm focal length) onto the entrance slit of a Jobin-Yvon spectrometer (1.5 m focal length, 1200 lines/mm holographic grating), equipped with an optical multichannel analyser (OMA). This OMA has a detector array which is divided into 512 channels (EG&G 1455R-512-HQ). The dispersion was 12.59 pm/channel at 589.0 nm in first order of diffraction. The spectrometer was very carefully calibrated in wavelength as well as in intensity (Aparicio et al. 1997). Time exposures for the spectra were 5 μs. Mirror M 3, placed behind the plasma column, was used to measure the optical depth and to detect possible self-absorption effects on each line profile. This can be done by comparing the spectra taken with and without the light reflected by this mirror.

3. Measurements and plasma diagnostics

The experiment consists of end-on measurements of the NII lines emitted by the plasma in the region 380−700 nm, and also the NI lines 742.36, 744.23 and 746.83 nm. Each spectral interval has been recorded at 15 different instants of the plasma lifetime. For each instant, we have made six runs, three of them with the mirror M 3 and the other three ones without it, in order to test for self-absorption in all measurements. The averages of the 3 registers made without mirror M 3 differed from the measured spectra less than 4%, which indicates the great repeatability of this plasma source. By comparing the average of registers with the mirror with the average of the registers without it and using the algorithms described in (González 1999) self-absorption only appeared in less than 2% of the whole spectral profiles. Even more, in less than 10% of these cases, the original profiles which can be reconstructed had peak intensity greater than 1.2 times that measured without mirror M 3. In these cases, the profile was rejected for further calculations. An example of a spectrum recorded with several NII lines at 50 μs of the plasma life is shown in Fig. 2.

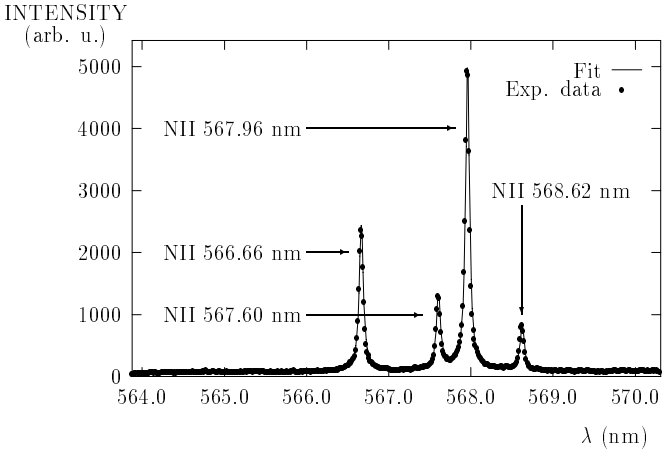

Fig. 2. An example of experimental spectrum showing several NII lines at the instant 50 μs of the plasma lifetime

It has also been possible to make measurements of the HeI 471.3 nm profiles, whose well-known Stark broadening has allowed us to determine the electron density spectroscopically. All the lines here considered were registered in first order of diffraction of the spectrometer, the most efficient. As a whole around 10000 discharges were made.

In relation to interferometric registers, 450 interferograms for both wavelengths were taken at the beginning, in the middle and at the end of the whole experiment. Besides, at regular intervals of 1.5 hours, 15 interferograms were registered, all of them 500 μs long. They have been used to determine the electron density evolution curve and to detect possible drifts in such a long experiment. When comparing the different curves, differences were always lower than 5%, which shows that no significant drifts occurred. This has also been shown when comparing temperature curves obtained from different groups of lines by means of Boltzmann-plots, each group corresponding to regular time intervals around 2 hours within the whole experiment. In fact, differences between temperature curves are also less than 5%. Anyway we have taken in each case for further calculations its corresponding temperature and density curve.

After dividing the spectra by the spectrometer transmittance functions, all the spectra were fitted to sums of Lorentzian functions plus a luminous background with a linear dependence, as explained in reference (Gigosos et al. 1994). Differences between the experimental spectra and the fits were usually lower than 1% (see Fig. 2). This fitting algorithm allows to determine simultaneously the center, asymmetry, linewidth and area of each profile.

Figure 3 shows the electron density N_e, determined interferometrically and spectroscopically. As it is shown in this figure, very good agreement between both methods is observed. Uncertainty in this plasma parameter is lower than 10%.

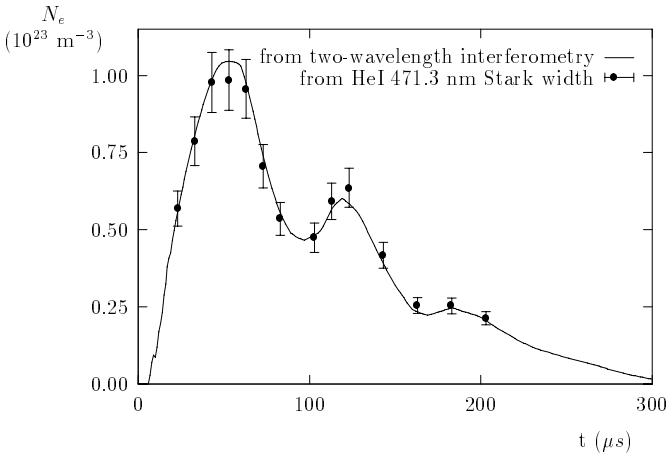

Fig. 3. Comparison between interferometric and spectroscopic electron density values. The uncertainty for this plasma parameter are below 10%

In collision-dominated plasmas like the one generated in this experiment, it is a common hypothesis to assume that excitation temperature, Saha temperature and kinetic electron temperature take similar values (Van der Mullen 1990). In this work excitation temperature has been calculated from NII Boltzmann-plots. As Fig. 4 shows, these plots involve NII lines whose upper energy levels cover a very broad range (from 20.64 to 30.36 eV). Here, for temperature determination, we introduce a fairly large number of lines, that is, of A_{ki} values taken from literature (the last data tabulated by NIST), which in fact will determine the absolute scale of this work A_{ki} data. In this way, the accuracy of this work results comes both from the great number of literature collected data as the great number of measurements taken into account in the temperature calculation. Additional determination of temperature was obtained from the NII/NI intensities ratio by combining different NII and the NI measured lines. The statistical error of temperature calculated from Boltzmann-plot is less than 5% (with the exception of the three last instants of plasma life, which is 7%). In the case of the temperature calculated from the intensity ratios this error does not exceed 3%. When combining intensities of consecutive species to calculate temperatures, total LTE is assumed and the measured electron density is used. As it can be seen in Fig. 5, the two methods employed in this experiment give rise to temperatures which cannot be distinguished into a very reasonable error band around 10%. Therefore, the assumption of a partial LTE model in the NII energy levels range considered can be perfectly made.

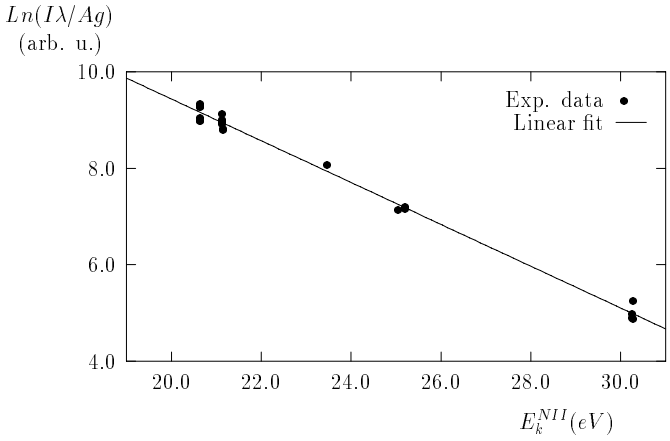

Fig. 4. An example of NII Boltzmann-plot corresponding to the plasmalife instant 50 μs. The good point distribution along the straight line shows that excitation temperature follows the Boltzmann law for these energy levels

4. Results and conclusions

Table 1 summarizes this work result, including the ratios with the literature collected values.

The uncertainty for each A_{ki} value of this experiment which can be estimated by the standard deviation that shows the different 15 experimental values for each line, is showed in percentages. Although with a clear dependence

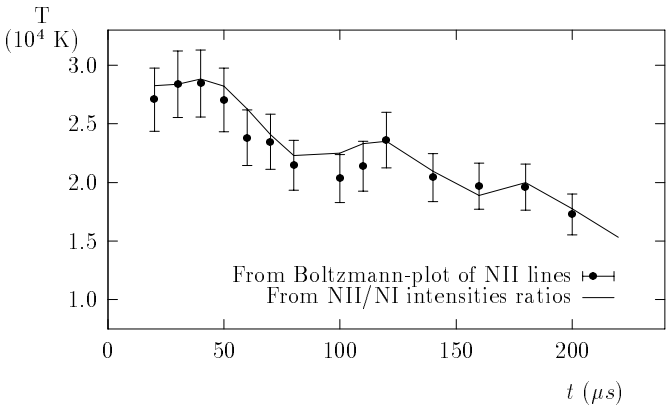

Fig. 5. NII excitation temperature evolution obtained from Boltzmann-plot and temperature curve obtained from NII/NI intensities ratio assuming total LTE. Although the statistical errors are below 5% in both methods, we give error bars up to 10% in order to include also the uncertainties coming from the set of A_{ki} data taken as reference from NIST critical compilation

on the line, usually uncertainties in this work are around 10%. For instance, Fig. 6 shows the different A_{ki}-values measured for two NII measured lines.

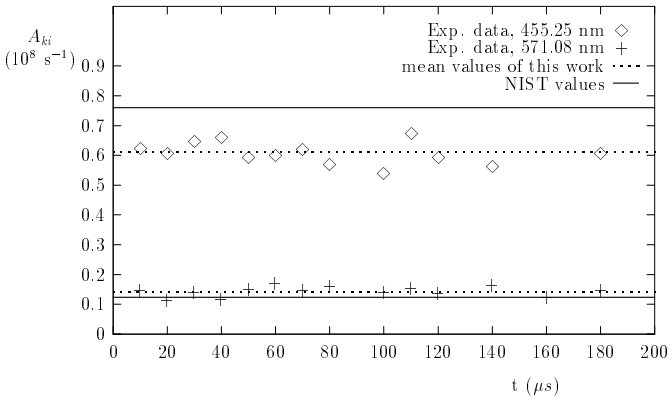

Fig. 6. An example of A_{ki} data of this work versus time of the plasma life for two NII lines. No trends are observed. The data of NII 571.08 nm line are in good agreement within 10% uncertainties with the NIST value compiled by Wiese et al. 1996 (with 3% accuracy). In the case of NII 455.25 nm line this work data (also with uncertainty of 10%) show differences around 20% with available NIST value. This can be explained taking into account that NIST data base value is within 30% accuracy in this case

Figure 7 shows the relative differences between the NIST values taken from literature as reference to determine NII excitation temperature from Boltzmann-plots, and this work for each line, as a function of wavelength. As can be seen, almost 80% of the data show differences below 15%. Usually NIST critical compilation assigned uncertainties around 10% to their values (in some cases around 30%). Taking into account this uncertainty and the statistical uncertainties assigned to each line in this work, the agreement is good. Also, Fig. 7 shows that there is no systematic trends in this experiment with wavelength, which gives an idea of the good spectral intensity calibration performed.

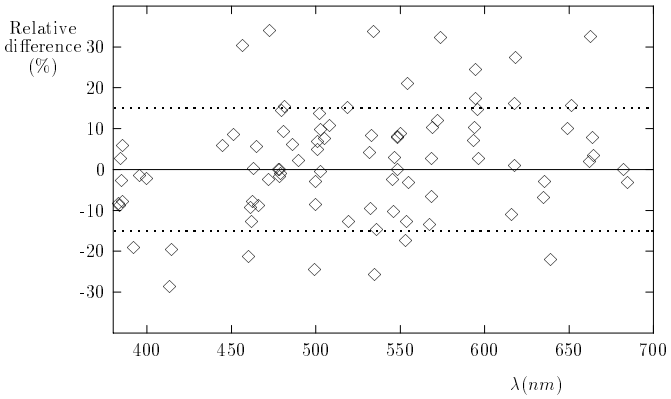

Fig. 7. Relative differences between this work A_{ki} values and NIST tabulated ones, taken as reference, versus λ. No trends are detected and 77% of the data differ less than 15%

As to the other literature collected data, the agreement is also good. The uncertainties of Musielok et al. work are also around 10%, while the differences with theoretical values reported by Lavin et al. (1999) working with a Relativistic Quantum Defect Orbital (RQDO) method with explicit polarization correction are also within a 10% error band. As can be seen in the table, the ratios between this work values and those of Musielok et al. tend to be systematically different within some multiplets. Greater in the ^{3}P $-^3$ D^0 multiplet of the 3p−3d transitions, and lower in the ^{3}P^0 $-^3$ P multiplet of the 3s−3p transitions. These tendencies are not so clear in ratios with NIST data. Perhaps differences could be partially explained by the different method used by Musielok et al. to put their measured line data on an absolute basis. Anyway, the very careful spectral calibration used in this work excludes systematic errors due to wavelength dependencies.

The 7 values quoted with * in the column Tw/NIST need a special comment. Although they have been obtained from NIST Standard Reference Database 61 (1995), with the following reference: Fuhr J. & Wiese W.L. "Atomic Transition Probabilities" in the CRC Handbook of Chemistry and Physics, chapter 10, (ed.) D.R. Lide (1995), they do not appear reflected in the Wiese et al. (1996) critical compilation. Besides NIST Database has assigned 30% uncertainties to these 7 lines. So they have not been used in the Boltzmann-plot temperature calculations in the present work. Their results show the greatest discrepancies. In the case of NII 405.69 nm line, this work result differ by a factor greater than 8. Perhaps an edition mistake in one order of magnitude could explain this.

As conclusion the main advantages of this experiment are the following:

a) About the 75% of the 95 spectral lines, whose data can be compared, agree both with the recent theoretical and experimental available data, assuming error bands around 10% in the considered works;

b) This work shows the coherence of a unique emission experiment, very carefully performed and with a good plasma diagnostics, which furnishes a great number of data for each line, and that for many lines;

c) Finally, this experiment improves the knowledge of A_{ki}-values for 13 new lines where we have not found previous references.

Acknowledgements. We thank S. González for his work in the experimental device. the Dirección General de Investigación Científica y Técnica (Ministerio de Educación y Ciencia) of Spain for its financial support under Contract No. PB-98-0356. and also the Consejería de Educación y Cultura de la Junta de Castilla y León (VA23-99). Dr. J.A. Aparicio wants to express his personal acknowledgement to the Organización Nacional de Ciegos de Espana (ONCE) for its help.

References

Aparicio J.A., Gigosos M.A., Mar S., 1997, J. Phys. B 30, 3141

Aparicio J.A., Gigosos M.A., González V.R., Pérez C., de la Rosa I., Mar S., 1998, J. Phys. B 31, 1029

del Val J.A., Mar S., Gigosos M.A., de la Rosa I., Pérez C., González V., 1998, Jpn. J. Appl. Phys. 37, 4177

Gigosos M.A., Mar S., Pérez C., de la Rosa I., 1994, Phys. Rev. E 49, 1575

González V.R., 1999, Ph.D. Thesis, Universidad de Valladolid

Lavín C., Olalla E., Martín I., 1999 (private communication)

Musielok J., Bridges J.M., Djurović S., Wiese W.L., 1996, Phys. Rev. A 53, 3122

Van der Mullen J.A.M., 1990, Phys. Rep. 191, 109

Wiese W.L., Fuhr J.R., Deters T.M., 1996, J. Phys. Chem. Ref. Data, Monograph 7. AIP, New York

Table 1. A_{ki}-values from this work arranged by wavelength. All values must be multiplied by 10^8 s^{-1}, and uncertainties σ are given in percentage. In the last three columns appear ratios between this work results Tw, and the available literature: NIST tabulated data by Wiese et al. (1996), Experimental data of Musielok et al. (1996) and theoretical calculations by RQDO treatment of Lavín et al., private communication (1999)

λ (nm)	Transition	Multiplet	$J_i - J_k$	A_{ki} This work	σ (%)	$Tw/NIST$ ratio	$Tw/Musielok$ ratio	$Tw/RQDO$ ratio
382.98	3p−4s	$^3P - ^3P^0$	1 − 2	0.223	16	0.92		
383.84	3p−4s	$^3P - ^3P^0$	2 − 2	0.639	6	0.92		
384.22	3p−4s	$^3P - ^3P^0$	0 − 1	0.314	11	1.03		
384.74	3p−4s	$^3P - ^3P^0$	1 − 1	0.216	12	0.97		
385.51	3p−4s	$^3P - ^3P^0$	1 − 0	0.935	20	1.06		
385.61	3p−4s	$^3P - ^3P^0$	2 − 1	0.343	7	0.93		
391.90	3p−3d	$^1P - ^1P^0$	1 − 1	0.559	10	0.83		0.73
395.59	3s−3p	$^3P^0 - ^1D$	1 − 2	0.129	11	0.99	0.97	
399.50	3s−3p	$^1P^0 - ^1D$	1 − 2	1.320	11	0.98		1.01
402.61	3d−4f	$^3F^0 - G(9/2)$	3 − 4	0.672	15	0.75*		
403.51	3d−4f	$^3F^0 - G(7/2)$	2 − 3	1.300	7			
404.13	3d−4f	$^3F^0 - G(9/2)$	4 − 5	2.080	10	0.79*		
404.35	3d−4f	$^3F^0 - G(7/2)$	3 − 4	1.250	25	0.51*		
404.48	3d−4f	$^3F^0 - G(7/2)$	3 − 3	0.214	39			
405.69	3d−4f	$^3F^0 - G(7/2)$	4 − 4	0.199	20	0.12*		
407.30	3d−4f	$^3F^0 - F(7/2)$	2 − 3	0.499	19			
407.69	3d−4f	$^3F^0 - F(5/2)$	2 − 2	0.080	42			
408.23	3d−4f	$^3F^0 - F(7/2)$	3 − 4	0.335	16			
413.18	3d−4f	$^1D^0 - G(7/2)$	2 − 3	0.204	13			
413.37	3s−3p	$^5P - ^5S^0$	2 − 2	0.398	11	0.75		
414.58	3s−3p	$^5P - ^5S^0$	3 − 2	0.605	15	0.82		
417.16	3d−4f	$^1D^0 - F(7/2)$	2 − 3	0.448	11			
417.36	3d−4f	$^3D^0 - D(5/2)$	2 − 2	0.120	30			
417.62	3d−4f	$^1D^0 - F(5/2)$	2 − 3	1.130	19	0.52*		
417.97	3d−4f	$^3D^0 - D(5/2)$	3 − 3	0.470	23			
441.71	3d−4f	$^3P^0 - D(3/2)$	2 − 2	0.233	14			
442.72	3d−4f	$^3P^0 - D(3/2)$	1 − 2	0.568	50			
444.20	3d−4f	$^3P^0 - D(5/2)$	1 − 2	0.695	16			
444.70	3p−3d	$^3D - ^3D^0$	1 − 2	1.210	9	1.06		0.93
450.76	3p−3d	$^3D - ^3P^0$	3 − 2	0.109	6	1.09		
453.04	3d−4f	$^1F^0 - G(9/2)$	3 − 4	1.450	20	0.86*		
455.25	3d−4f	$^1F^0 - G(7/2)$	3 − 4	0.611	9	0.80*		
456.48	3p−3d	$^1P - ^3F^0$	1 − 2	0.019	16	1.36		
460.15	3s−3p	$^3P^0 - ^3P$	1 − 2	0.190	9	0.81	0.69	0.86
460.72	3s−3p	$^3P^0 - ^3P$	0 − 1	0.297	8	0.91	0.76	0.95
461.39	3s−3p	$^3P^0 - ^3P$	1 − 1	0.199	4	0.88	0.74	0.91
462.14	3s−3p	$^3P^0 - ^3P$	1 − 0	0.882	8	0.92	0.80	0.95
463.05	3s−3p	$^3P^0 - ^3P$	2 − 2	0.775	7	1.00	0.88	1.12
464.31	3s−3p	$^3P^0 - ^3P$	2 − 1	0.477	7	1.06	0.94	1.25
465.45	3s−3p	$^1P^0 - ^3P$	1 − 2	0.022	11	0.92	0.82	
469.46	3d−4f	$^1P^0 - D(5/2)$	1 − 2	0.607	12			
471.84	3p−3d	$^5D^0 - ^5D$	4 − 4	0.295	4	0.98		
472.16	3p−3d	$^5D^0 - ^5D$	4 − 3	0.110	11	1.41		
477.42	3p−3d	$^3D - ^3D^0$	1 − 2	0.032	11	1.00	0.82	0.80
477.97	3p−3d	$^3D - ^3D^0$	1 − 1	0.248	6	0.98	1.06	0.91
478.12	3p−3d	$^3D - ^3D^0$	2 − 3	0.021	12	1.00	0.84	0.70
478.81	3p−3d	$^3D - ^3D^0$	2 − 2	0.250	5	0.99	0.97	1.00
479.37	3p−3d	$^3D - ^3D^0$	2 − 1	0.090	5	1.15	1.06	1.00
480.33	3p−3d	$^3D - ^3D^0$	3 − 3	0.349	4	1.10	1.02	1.09
481.03	3p−3d	$^3D - ^3D^0$	3 − 2	0.056	14	1.17	1.02	1.00
486.02	3p−3d	$^3D - ^1D^0$	1 − 2	0.017	5	1.06		
489.51	$2p^3$−3p	$^1D^0 - ^1P$	2 − 1	0.044	15	1.02		

Table 2. Continued from Table 1

λ (nm)	Transition	Multiplet	$J_i - J_k$	A_{ki} This work	σ (%)	$Tw/NIST$ ratio	$Tw/Musielok$ ratio	$Tw/RQDO$ ratio
498.74	3p−3d	^{3}S $-^3$ P^0	1 − 0	0.586	13	0.78	0.78	
499.12	3s−3p	^{5}P $-^5$ P^0	1 − 2	0.325	35	0.92		
499.44	3p−3d	^{3}S $-^3$ P^0	1 − 1	0.738	5	0.97	0.96	0.98
500.51	3s−3p	^{5}P $-^5$ P^0	2 − 2	1.220	7	1.05	0.95	0.97
500.73	3p−3d	^{3}S $-^3$ P^0	1 − 2	0.844	8	1.07	1.08	1.13
501.64	3p−3d	^{3}D $-^3$ F^0	2 − 2	0.186	5	1.15	1.01	0.96
502.30	3s−3p	^{5}P $-^5$ P^0	3 − 2	0.359	15	0.99		
502.57	3p−3d	^{3}D $-^3$ F^0	3 − 3	0.118	11	1.10	1.01	1.15
504.51	3s−3p	^{3}P^0 $-^3$ S	2 − 1	0.369	8	1.08	1.11	0.98
507.36	3s−3p	^{1}P^0 $-^3$ S	1 − 1	0.029	7	1.12	1.07	
518.32	3p−3d	^{5}P^0 $-^5$ D	3 − 3	0.335	30	1.16		
519.04	3p−3d	^{5}D^0 $-^5$ F	4 − 4	0.156	16	0.88		
531.34	3p−3d	^{5}P^0 $-^5$ P	1 − 1	0.147	8	1.04		
532.02	3p−3d	^{5}P^0 $-^5$ P	2 − 1	0.382	15	0.91		
532.10	3p−3d	^{5}P^0 $-^5$ P	1 − 2	0.274	11	1.09		
533.87	3p−3d	^{5}P^0 $-^5$ P	2 − 3	0.260	13	1.41		
534.02	3p−3d	^{5}P^0 $-^5$ P	3 − 2	0.200	21	0.77		
535.12	3p−3d	^{5}P^0 $-^5$ P	3 − 3	0.317	19	0.86		
545.21	3p−3d	^{3}P $-^3$ P^0	0 − 1	0.087	12	0.98	1.09	0.78
545.42	3p−3d	^{3}P $-^3$ P^0	1 − 0	0.302	6	0.90	0.98	0.90
546.26	3p−3d	^{3}P $-^3$ P^0	1 − 1	0.103	6	1.03	1.08	1.23
547.53	3s−4p	^{1}D^0 $-^1$ D	2 − 2	0.047	32	1.00		
547.81	3p−3d	^{3}P $-^3$ P^0	1 − 2	0.052	11	1.08	1.11	0.63
548.01	3p−3d	^{3}P $-^3$ P^0	2 − 1	0.141	7	1.09	1.24	1.01
549.57	3p−3d	^{3}P $-^3$ P^0	2 − 2	0.262	5	1.09	1.16	1.06
552.62	3s−3p	^{5}P $-^5$ D^0	1 − 2	0.179	13	0.84		
553.02	3s−3p	^{5}P $-^5$ D^0	2 − 3	0.356	18	0.88		
554.01	3s−3p	^{5}P $-^5$ D^0	1 − 2	0.745	19	1.24		
554.35	3s−3p	^{5}P $-^5$ D^0	2 − 2	0.340	11	0.97		
566.66	3s−3p	^{3}P^0 $-^3$ D	1 − 2	0.327	10	0.87	1.00	0.91
567.60	3s−3p	^{3}P^0 $-^3$ D	0 − 1	0.304	6	1.03	1.13	1.15
567.96	3s−3p	^{3}P^0 $-^3$ D	2 − 3	0.492	9	0.94	1.02	1.04
568.62	3s−3p	^{3}P^0 $-^3$ D	1 − 1	0.215	10	1.11	1.21	1.09
571.08	3s−3p	^{3}P^0 $-^3$ D	2 − 2	0.140	10	1.13	1.23	1.19
573.07	3s−3p	^{3}P^0 $-^3$ D	2 − 1	0.018	12	1.39	1.29	1.39
592.78	3p−3d	^{3}P $-^3$ D^0	0 − 1	0.346	3	1.08	1.23	1.33
593.18	3p−3d	^{3}P $-^3$ D^0	1 − 2	0.473	4	1.11	1.33	1.34
594.02	3p−3d	^{3}P $-^3$ D^0	1 − 1	0.289	7	1.28	1.74	1.48
594.17	3p−3d	^{3}P $-^3$ D^0	2 − 3	0.659	5	1.19	1.41	1.41
595.24	3p−3d	^{3}P $-^3$ D^0	2 − 2	0.147	5	1.16	1.47	1.27
595.43	3d−4p	^{1}P^0 $-^1$ S	1 − 0	0.508	14	1.03		
615.08	3d−4p	^{3}F^0 $-^3$ D	2 − 2	0.026	4	0.90		
616.78	3d−4p	^{3}F^0 $-^3$ D	4 − 3	0.311	9	1.17		
617.02	3d−4p	^{3}F^0 $-^3$ D	2 − 1	0.288	14	1.01		
617.33	3d−4p	^{3}F^0 $-^3$ D	3 − 2	0.345	12	1.32		
634.06	3d−4p	^{3}D^0 $-^3$ P	3 − 2	0.199	16	0.93		
634.69	3d−4p	^{3}D^0 $-^3$ P	1 − 1	0.067	20	0.97		
637.96	3s−3p	^{3}P^0 $-^1$ P	1 − 1	0.049	10	0.80	0.80	
648.21	3s−3p	^{1}P^0 $-^1$ P	1 − 1	0.333	7	1.11		1.03
650.46	3d−4p	^{3}D^0 $-^3$ D	3 − 3	0.062	10	1.17		
661.06	3p−3d	^{1}D $-^1$ F^0	2 − 3	0.647	10	1.02		1.01
661.36	4s−3s	^{3}P^0 $-^3$ P	2 − 2	0.219	34	1.39		
662.98	3d−4p	^{1}D^0 $-^1$ P	2 − 1	0.291	19	1.08		
663.48	4s−3s	^{3}P^0 $-^3$ P	2 − 1	0.091	10	1.03		
681.00	3d−4p	^{3}P^0 $-^3$ S	2 − 1	0.231	6	1.00		
683.41	3d−4p	^{3}P^0 $-^3$ S	1 − 1	0.158	21	0.97		